Detection of neutral beam deuterons acceleration by 2nd harmonic radio frequency heating in ASDEX Upgrade via neutron spectrometry

G. Tardini‡, R. Bilato, R. Fischer, M. Weiland, and the ASDEX Upgrade Team

Max-Planck-Institut für Plasmaphysik, Boltzmannstraße 2, 85748 Garching, Germany

Abstract. Second harmonic absorption of radio frequency in the Ion Cyclotron Range of Frequency (ICRF) by fast D is expected in the case of H minority heating at the fundamental cyclotron frequency, provided the ion Larmor radius is of the order of the RF-wavelength, as it is for Neutral Beam Injection (NBI)-D ions. In tokamaks a strong increase of neutron production is observed when such an ICRF heating is applied on top of NBI, often referred to as "synergy effect".

On ASDEX Upgrade a scintillator-based Compact Neutron Spectrometer (CNS) is available outside the torus hall, with perpendicular view through the plasma equatorial plane, measuring Pulse Height Spectra (PHS), which allow to infer the ion distribution functions, in particular the suprathermal tail.

The measured PHS exhibit clear energetic tails when ICRF is applied in the presence of NBI, proving there's an overproportional tail in the fast-ion distribution at the high energy end. The PHS in the CNS line-of-sight are modelled coupling kinetic

‡ Corresponding author: git@ipp.mpg.de

solvers with wave codes. Unfolding the PHS into neutron emission spectra allows to quantify the maximum fast ion energy with significant occurrence, showing a non-negligible population around 500 keV, significantly higher than the NBI energy. A sensitivity study assesses the maximum fast ion energy compatible with the measured PHS, confirming the presence of 500 keV D ions.

Keywords: Neutron spectrometry, scintillator, pulse height spectrum, ICRF, kick operator

1. Introduction

A typical heating scheme for tokamak D plasmas with Radio-Frequency (RF) waves is based on the excitation of the fast-wave in the Ion Cyclotron Range of Frequencies (ICRF) for the H minority at the fundamental cyclotron frequency. In presence of high T_i or significant suprathermal D population, there is a finite absorption by D (majority) at the 2nd harmonic, which is a Finite Larmor Radius (FLR) effect, if the ion Larmor radius is comparable to the RF wavelength. In the case of NBI heated plasmas, this effect is expected to be significant, because the ion Larmor radius scales like $\sqrt{E_D}$, E_D being the D-ion energy. Until recently, the massive increase of neutron production rate was the main experimental evidence for ICRF D acceleration at higher harmonics [1][2]. However, spectrospic measurements have added significant energy-resolved evidence of energetic ions beyond the injection energy at JET, first for third-harmonic acceleration of D [3][4][6][7][8] and very recently also for second-harmonic [9][10]. For the first time, such evidence both on the experimental and on the modelling side is found for the tokamak ASDEX Upgrade too.

A comprehensive set of fast ions diagnostics in ASDEX Upgrade allows now a direct measurement of the suprathermal D population [11]. The Neutron Emission Spectrum (NES) contains information on the fast ions distribution function, because fusion neutrons are Doppler shifted depending on the velocities of the reacting deuterons [12][13][14]. On ASDEX Upgrade a Compact Neutron Spectrometer (CNS) is available, based on the liquid organic scintillator BC501a (former NE213) [15] [16]. A photo-

multiplier collects and amplifies the scintillation signal which is then digitalised with a Digital Acquisition system [17] and then processed software-wise to discriminate gamma from neutron events via Digital Pulse Shape Discrimination [18][19][15]. The detector collects the light produced by recoil protons. Since a proton can receive any energy between zero and the incoming neutron energy in the elastic scattering process, and the detector response is energy dependent, the NES are convoluted with the detector response function: the directly measured quantity is, in fact, the Pulse Height Spectrum (PHS). Details about the detector, the acquisition board and the discrimination algorithm can be found in [15].

2. Strong increase of the neutron rate

As observed in the past, adding ICRF heating with H-minority absorption at the fundamental frequency in the plasma core in a NBI-heated plasma produces a strong increase of the neutron rate. We designed a few plasma dischrages in ASDEX Upgrade with particularly long slowing-down time, to maximise the fast particle density and average energy. In order to operate at low density, the plasma current was taken to be low (0.6 MA), moreover we restricted to just one NBI source (2.5 MW, central heating) to minimise the particle source. The resulting plasma density was $\sim 5\ 10^{19} m^{-3}$. The magnetic field was 2.5 T. The ICRF input was maximised with ~ 5 MW of nominal power, corresponding to ~ 4 MW coupled to the plasma. The heating scheme was H-minority, with a 180 degree (dipole) antenna phasing and $n_H/n_e \approx 5\%$. As a

consequence, a significant power fraction is absorbed by the H minority. The time traces of discharge #29795 are summarised in Figure 1, featuring the strong increase of the neutron rate as soon as ICRF is aplied on top of NBI heating. The neutron rate,

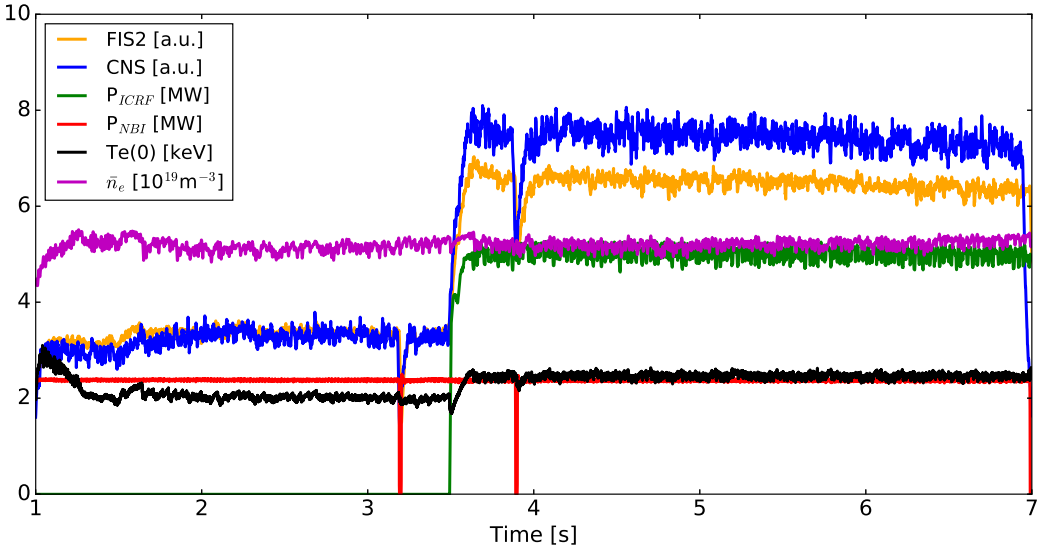

Figure 1. Time traces for discharge # 29795. The neutron rates FIS2 and CNS are uncalibrated signals, here they have been cross-normalised to match in the NBI-only phase.

before and after switching on the ICRF, is measured with two completely independent detectors, based on different principles: a fission chamber (FIS2) placed in a moderator in the torus hall next to the tokamak (orange trace in Fig. 1); the CNS located outside the torus hall (blue trace). The uncalibrated signals are rescaled to show the accurate agreement of the ratio between the neutron rate with ($= y_{NBI+IC}$) and without ICRF ($= y_{NBI}$). Both diagnostic systems measure an increase of the neutron rate by factors 1.5-3 when ICRF is switched on, for all analysed discharges (see blue and orange symbols in Fig. 7). As Fig. 2 shows, this cannot be simply explained with the observed change in

the kinetic profile, by modifying only the slowing down time. If no interaction of the wave with the suprathermal D population is assumed, the increase of the neutron rate simulated with the TRANSP code [28] is not significant, when ICRF is added at 3.5 s. Precisely, the increase is roughly a factor 2 in the experiment (Fig. 1) while it's only 1.1 in the simulation.

Note that for the modelled neutron production we can distinguish between thermonuclear, beam-beam and beam-target neutrons. Since beam-target reactions are dominant in the discharges analysed in this work (see red trace in Fig. 2), as already observed in ASDEX Upgrade NBI heated plasmas [20], the NES provides useful information for the fast ion energy distribution. The strong increase in neutron rate is

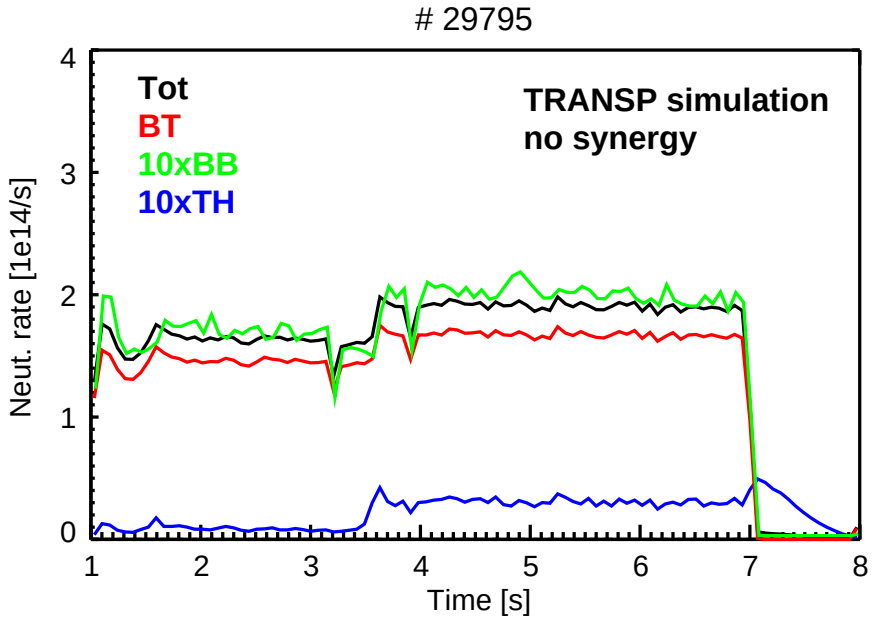

Figure 2. Neutron rate for discharge # 29795, simulated without any synergy model: total signal (black), beam-target (red), 10x thermonuclear (blue), 10x beam-beam (green). Beam-target reactions are 90% of the total yield.

a very robust and reproducible observation. It has been explained as direct absorption of RF waves by D-ions with a large Larmor radius, such as fast NBI-D ions [1][5]. This explanation seems confirmed by recent measurements with the Fast Ion D-Alpha (FIDA) diagnostics [11]. However, FIDA cannot measure accurately fast ions above energies of ~ 150 keV, due to the charge exchange cross-section having a maximum around 60 keV, thus reducing the signal-to-noise ratio at high energies [11]. Moreover, such an increase of the neutron rate could be explained also with a lesser sensitivity of NBI-D ions to turbulence or in general to a reduction of turbulent transport in presence of fast ions [22].

3. Energetic tails in Pulse Height Spectra and Neutron Emission Spectra

The CNS measures PHS, which corresponds roughly to the energy distribution of the recoil protons in the scintillator cell after the scattering with the incoming neutrons. A PHS is the convolution of the NES with the instrumental response functions [21]. In Fig. 3 we compare the PHS in the phase with NBI only (red) with the one in the NBI+ICRF phase (green line).

The PHS is unfolded into a NES, which contains information on the fast ion distribution. The deconvolution is performed using two codes, both based on the maximum entropy ansatz: the MAXED code [23] and the Deconvolution method with Adaptive Kernel (DAK) [24]. In Fig. 4 both unfolding methods show qualitatively and quantitatively similar NES. Note that there is some freedom in the unfolsing settings,

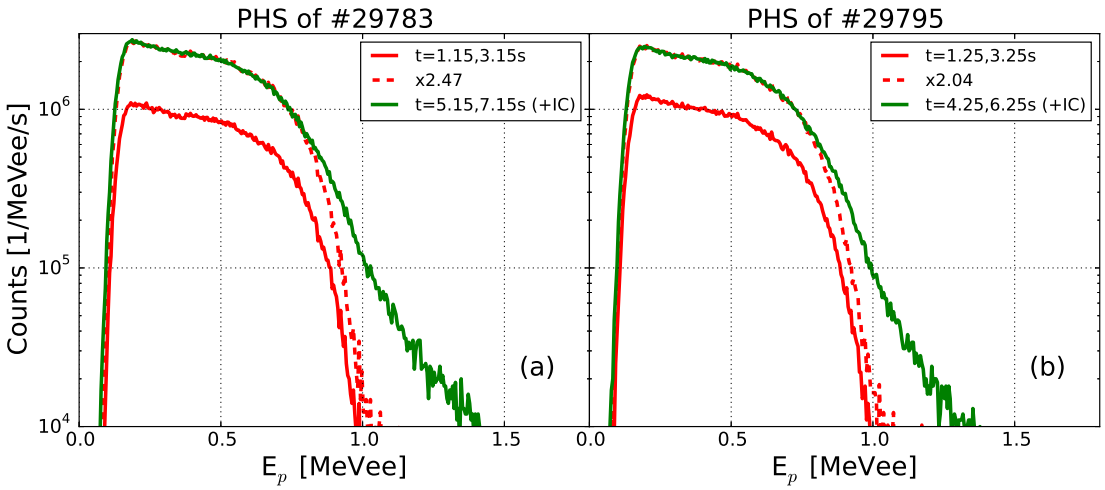

Figure 3. Semi-logarithmic plot of the PHS for discharges #29783 and #29795. NBI+ICRF phase (green) and NBI only phase (red): actual count (continuous) and rescaled (dashed).(a) #29783 (b) #29795.

for instance the degree of smoothness versus closeness to the measured PHS. Too little smoothing might add noise and artifacts, too much smoothing can eliminate real physics features. For the record, the MAXED unfolding in Fig. 4 (a) was done with a target χ^2 = 0.2 for both time intervals. Both codes assumed a Poisson uncertainty, i.e. the square root of the measured PHS. In the DAK code, such an uncertainty was then doubled, to optimise the trade-off between accuracy and smoothness, as the χ^2 is no input, it adapts to the prescribed uncertainty. The characteristic double peak feature associated with a perpendicular cone-of-sight is clearly visible. This is due to the projection of the NBI-D gyro-motion along the line-of-sight and it is expected and regularly observed in tokamaks [12][13]. The energetic tail is significant, the maximum neutron energy moves from $\sim$ 3 to $\sim$ 4 MeV when ICRF is added, proving that ions are accelerated beyond the NBI energy. A few artifacts are present at both the low and the high energy tail,

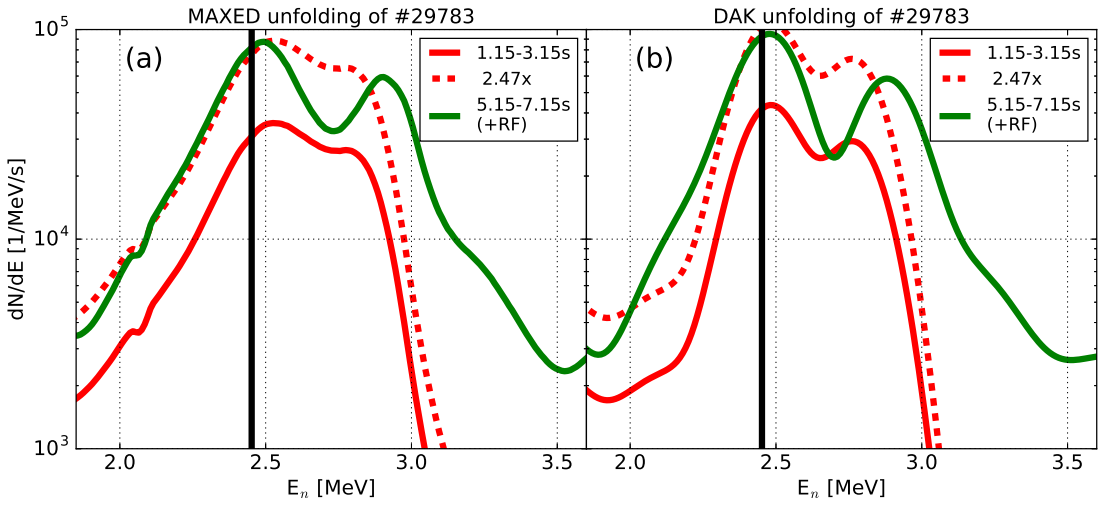

Figure 4. Semi-logarithmic plot of the NES for discharge#29783, unfolding the experimental PHS with the MAXED code. NBI+ICRF (green) and NBI only phase (red): original (continuous) and rescaled (dashed). Unfolding with the (a) MAXED and (b) DAK codes. The black vertical line is the reference neutron energy at rest from d-d fusion. The rescaling of the dashed line is taken as the PHS rescaling factor, see Fig. 3.

with both unfolding methods, due to the slightly hollow instrumental response [21]. Howevever, we can have an approximate estimate of the maximum fast ion energy by using the simple formula $\Delta E_n \approx \sqrt{E_{fus} E_{fi,max}}$, ΔE_n being $E_{max} - E_{fus}$; $E_{fus} = 2.45$ MeV is the reference neutron energy at rest from D-D reactions, $E_{fi,max}$ the maximum fast-ion energy, which is expected to be equal to $E_{NBI,inj}$ in case of pure NBI heating, whereas it has to be determined from the NES in case of D acceleration by ICRF. The formula for ΔE_n is derived from simple kinematics changing the reference frame, making use of $(v_{fus} + v_{fi,max})^2 \approx v_{fus}^2 + 2 v_{fus} * v_{fi,max}$. Substituting E_{fus} and $E_{fi,max} = 60$ keV, one obtains $\Delta E_n \approx 0.4$ MeV, consistent with the red distribution in Fig. 4. A $\Delta E_n \approx$

1.2 MeV, observed in the green curves of Fig. 4 (a) and (b) corresponds to $E_{fi,max} \approx$ 500 keV.

4. Modelling the NBI-ICRF synergy

The synergy effect between ICRF waves and a NBI-generated fast ion population has been recently modelled with different approaches. A quasi-linear RF-kick operator accounts for D acceleration in the MonteCarlo ansatz of TRANSP/NUBEAM [25], with a net momentum-trasfer to fast ions when they transit through the resonant region of the RF-field. The alternative approach is based on the TORIC+SSFPQL package [26][1]. TRANSP, on the one hand, follows the fast-ion orbits with a realistic collision operator, thus predicting fast ion losses and the slowing down process accurately and time-dependent. The TORIC+SSFPQL suite, on the other hand, has a consistent treatment of the back-reaction of the ICRF-NBI deformed distribution function onto wave-propagation and absorption.

According to both code packages, fast D-ions are accelerated well beyond the NB injection energy of 60 keV, as the comparison between Fig. 5 (a), (b) and (c) shows. Figure 5 (a) is the fast ion distribution function as modelled with TRANSP/NUBEAM before ICRF is applied; (b) is the case in the NBI+ICRF phase neglecting the RF-kick operator, which is instead included in (c). The fact that the fast ion distribution (a) and (b) are almost identical shows that the RF-kick operator is the most significant effect of the strong change in the distribution function when ICRF is applied. In fact

there is no significant fast ion population above the NB injection energy of 60 keV. Even

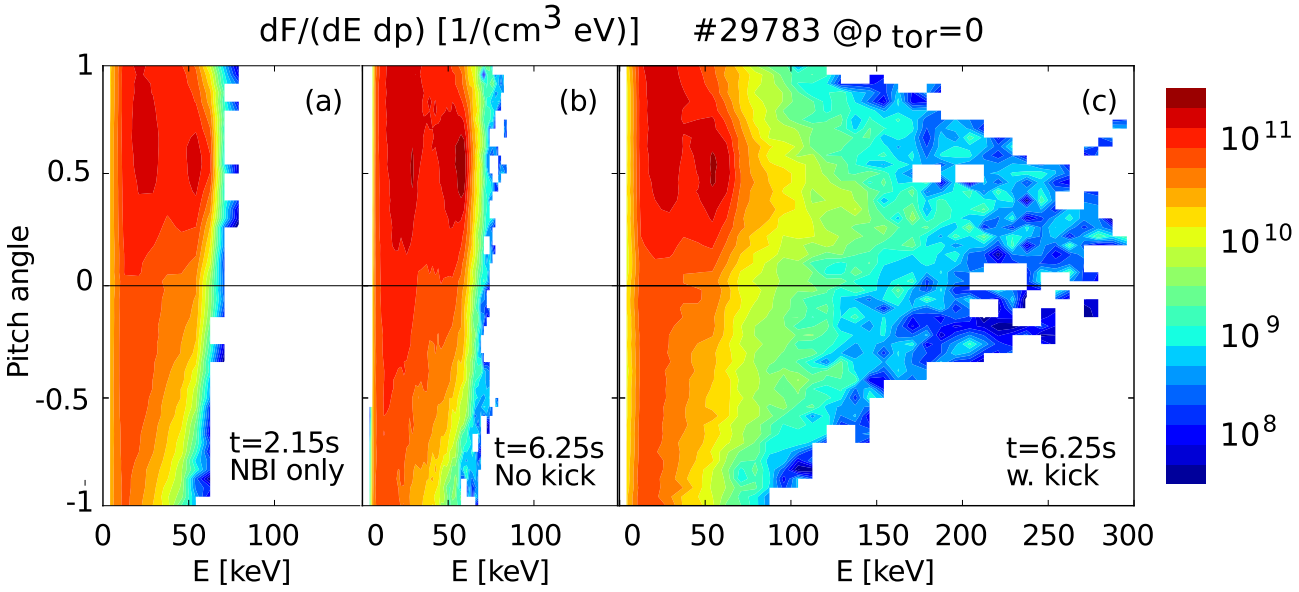

Figure 5. Energy/pitch fast ion distribution in the plasma center from TRANSP simulations. In the NBI-phase (a); in the NBI-ICRF phase, simulation without (b) and with RF-kick (c).

if the phase-space density of fast ions beyond 60 keV, as predicted including the RF-kick, Fig. 5 (c), is a few orders of magnitude lower than below 60 keV, such energetic ions contribute significantly to the plasma pressure and they are more likely to undergo fusion reactions, due to the positive energy-dependence of the d-d cross-sections [27]. A quantitative comparison with the neutron rates and spectra in the diagnostic's cone-of-sight is now possible.

4.1. Neutron rate simulation

In Fig. 6 we compare modelling results with and without RF-kick with experimental measurements, focussing on the increase at ICRF onset time. The RF-kick operator

is obviously necessary to reconcile the simulations with the experimental neutron rate. This is the case for all analysed discharges. We summarise such a ratio for several

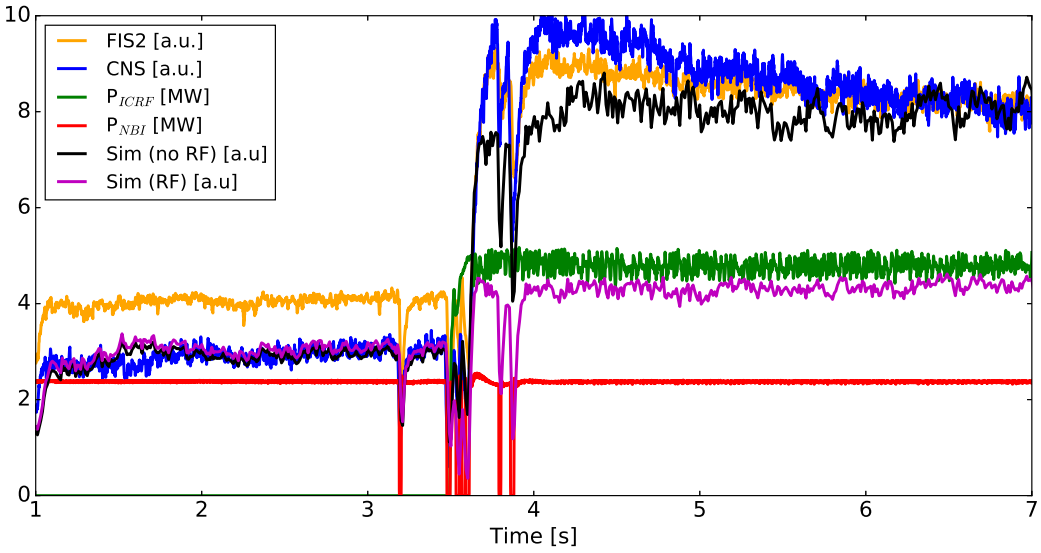

Figure 6. Measured and simulated neutron rates before and after switching on P_{ICRF} (green) on top of constant P_{NBI} (red): CNS (blue), FIS2 (orange), simulation with (black) and without RF-kick (magenta).

discharges and both diagnostics in Fig. 7. There is a considerable improvement in the agreement between measurement and simulation when including the RF-kick. The predicted ratio is accurate, in particular, when compared to the CNS measurement, which has a linear response over the whole relevant count rates' range - whereas FIS2 is not for rates above $\sim 3\ 10^{14}\ s^{-1}$.

4.2. Neutron spectra

The GENESIS code [29] allows to calculate NES in the realistic cone-of-sight of the CNS, providing a fast ion distribution such as the one calculated by TRANSP/NUBEAM

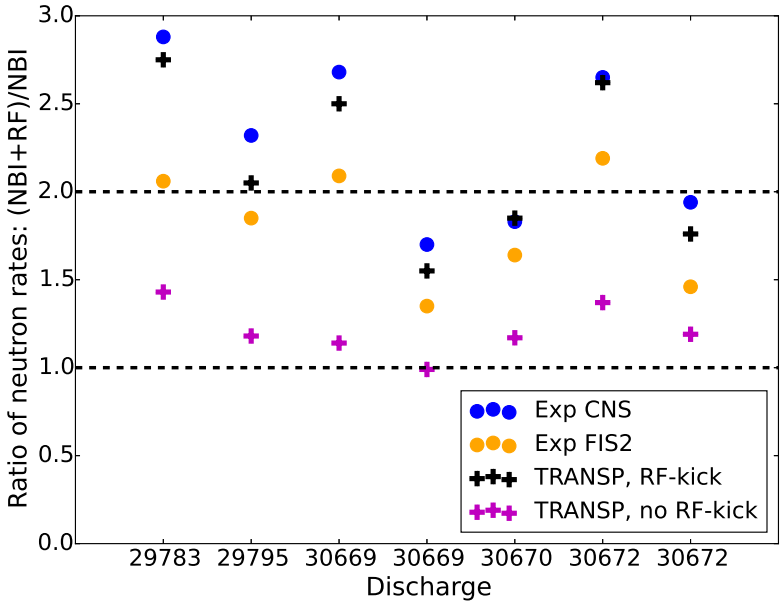

Figure 7. Measured and simulated ratio of neutron rates before and after switching on P_{ICRF} on top of constant P_{NBI}: CNS (blue), FIS2 (orange), TRANSP simulation with (black) and without RF-kick (magenta). Multiple time intervals are analysed for #30669 and #30672.

(Fig. 5) or by TORIC+SSFPQL. The simulation result is shown in Fig. 8. The modification of the NES (Fig. 4), both in scale and in shape, can be compared with the deconvolution of the experimental PHS. The variation is well predicted in the case of TRANSP/NUBEAM (Fig. 8 (a)) whereas the energetic tail is largely overpredicted for TORIC+SSFPQL (Fig. 8 (b)). A possible explanation is the missing fast ion transport in TORIC+SSFPQL, which leads to a more effective acceleration of already accelerated fast ions and hence to an overestimate of the neutron rate and of the high-energy tail of the fast ion population and of the NES. The same trend is, of course, found also when convolving the simulated NES with the instrument response function, for comparison

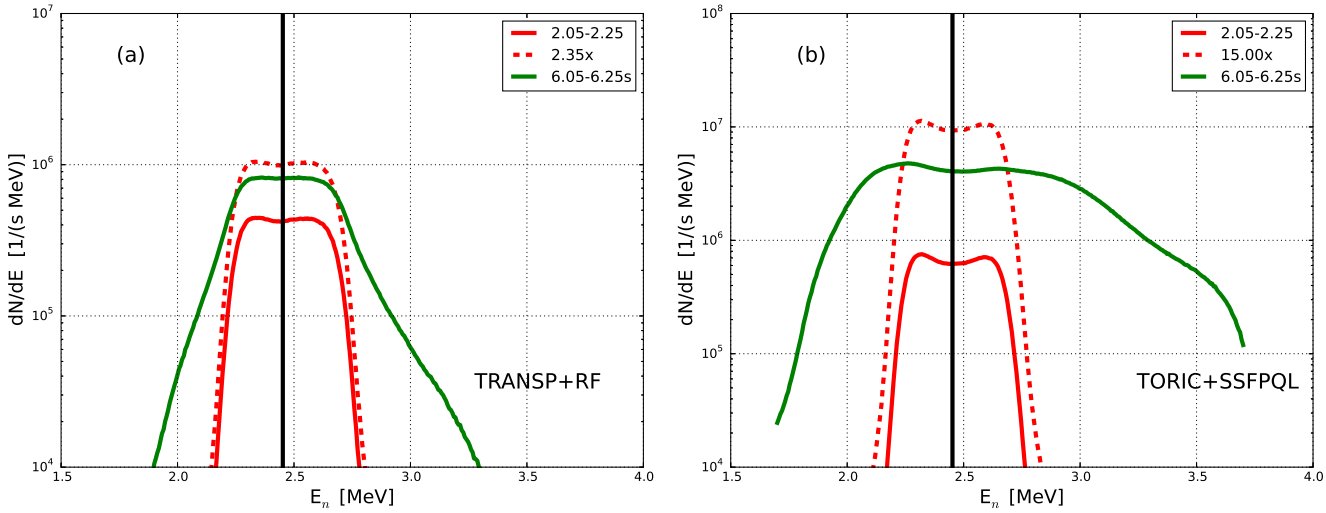

Figure 8. Semi-logarithmic NES for discharge # 29783 calculated with GENESIS from plasma simulations with a) TRANSP+RF b) TORIC+SSFPQL. NBI phase (red continous), multiplied by a factor (red dashed) for comparison with NBI+ICRF (green). The black vertical line is the reference neutron energy at rest from d-d fusion.

with the measured PHS of Figure 3. Again, the TRANSP/NUBEAM package with RF-kick gives an accurate prediction of the change in the PHS (Fig. 9 (a)), whereas TORIC+SSFPQL exhibits again a pronounced energetic tail (Fig. 9 (b)), consistently with Fig. 8.

4.3. Sensitivity study

A sensitivity study is performed, limiting the maximum energy of the TRANSP fast ion distribution. In Fig. 10 we plot the normalised NES and PHS corresponding to energy cuts at 60, 200 and 500 keV, as well as the cases without RF kick and with full distribution. The case with 60 keV is, as expected, overlapping the simulation without

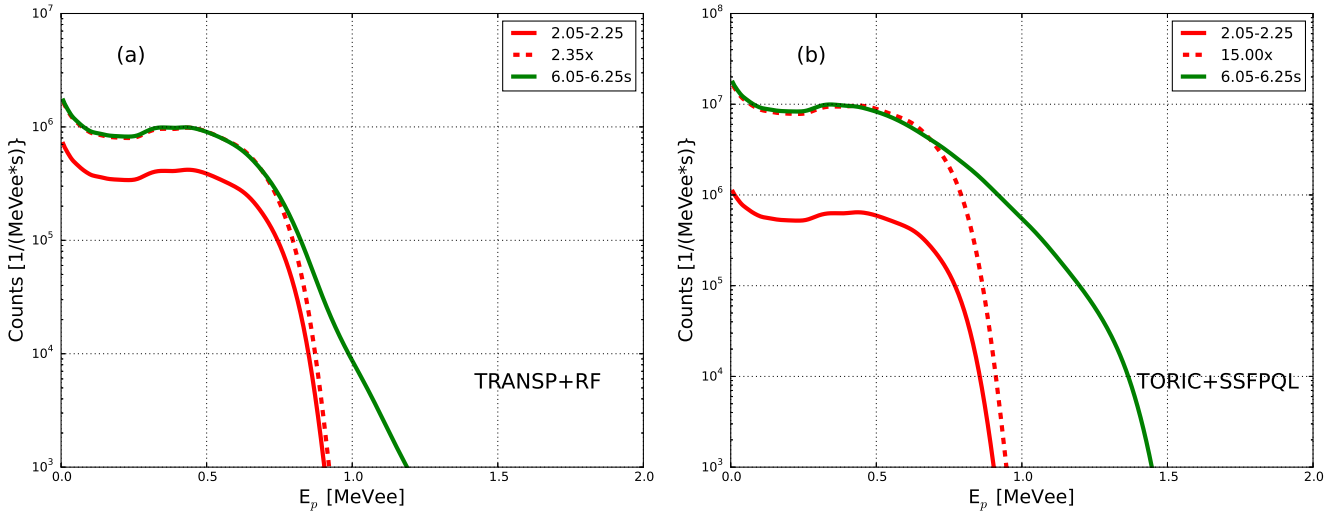

Figure 9. Semi-logarithmic PHS for discharge # 29783 folding the GENESIS calculations with the instrumental response function. Plasma simulations with a) TRANSP+RF b) TORIC+SSFPQL. NBI phase (red continous), multiplied by a factor (red dashed) for comparison with NBI+ICRF (green).

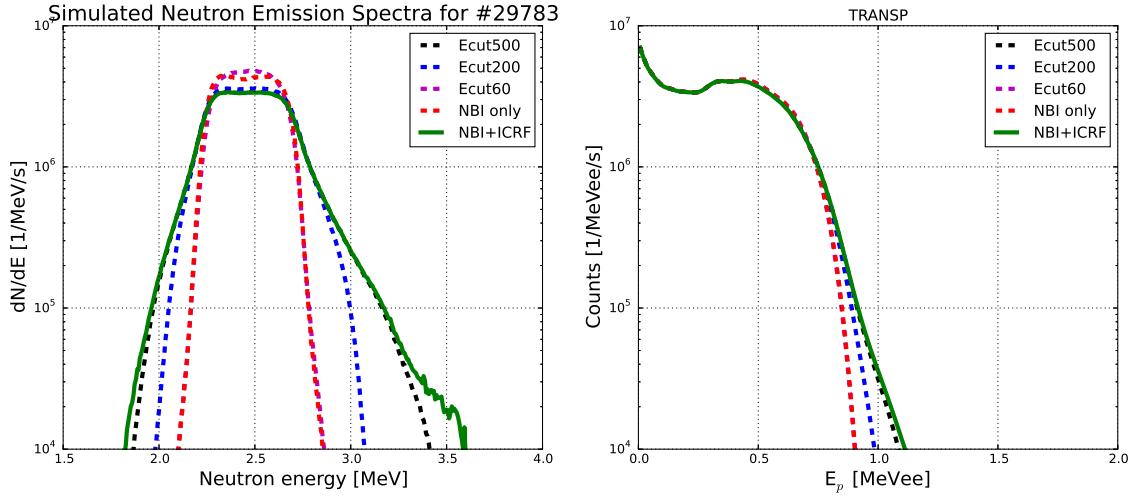

Figure 10. Sensitivity study for discharge # 29783 simulated with TRANSP+GENESIS cutting the fast ion energy. The rescaling has been determined as to match the plateau of the PHS.

RF-kick. To give a deviation from the NBI-only case comparable with the experimental evidence (Figures 3 and 4) energies of the order of 500 keV appear to be necessary.

5. Conclusions

The well-known synergy effect between ICRF and NBI, yielding a massive increase of the neutron production, is shown to be a direct consequence of the acceleration of deuterium at 2nd harmonic, confirming recent results for the JET tokamak [9][10], similarly to previous works on 3rd harmonic D-acceleration [3][4][5][6][7][8]. The measurements with the compact neutron spectrometer in ASDEX Upgrade provides experimental evidence for that, with a clear shape modification of the PHS towards energetic tails.

Modelling the effect by coupling plasma codes and neutron generation codes allows to assess quantitatively the effect: deuterium energy distributions featuring energetic tail up to 500 keV are observed, one order of magnitude higher than the NB injection energy. The deconvolution of the PHS into neutron emission spectra with two different unfolding methods (both based on entropy maximisation) confirms the fast ion energy around 500 keV, even though the spectra have uncertainties and a few artifacts.

Only the TRANSP simulation with RF-kick gives good quantitative prediction, while TORIC+ssfpql overpredicts strongly the neutron rate and the energetic tails of the PHS. This suggests that retaining fast ion transport and losses is important to prevent an exaggerated self-amplification of the fast ion acceleration, which becomes more effective as the Larmor radius of the fast D ion increases.

Acknowledgement

This work has been carried out within the framework of the EUROfusion Consortium and has received funding from the Euratom research and training programme 2014-2018 under grant agreement No 633053. The views and opinions expressed herein do not necessarily reflect those of the European Commission.

[1] R. Bilato *et al* , Nuclear Fusion **51** (2011) 103034

[2] L.-G. Eriksson *et al* , Nuclear Fusion **38** (1998) 265-278

[3] L. Giacomelli *et al* , Rev. Sci. Instrum. **79** (2008) 10E514

[4] D. Van Eester *et al* , Plasma Physics and Controlled Fusion **51** (2009) 044007

[5] E. Lerche *et al* , Plasma Physics and Controlled Fusion **51** (2009) 044006

[6] C. Hellesen *et al* , Nuclear Fusion **53** (2013) 113009

[7] J. Eriksson *et al* , Nuclear Fusion **55** (2015) 123026

[8] M. Schneider *et al* , Nuclear Fusion **56** (2016) 112022

[9] D. Gallart *et al* , Nuclear Fusion **56** (2016) 106037

[10] C. Hellesen *et al* , Nuclear Fusion **58** (2018) 056021

[11] M. Weiland *et al* , Nuclear Fusion **57** (2017) 116058

[12] M. Tardocchi, "Neutron emission spectroscopy studies of fusion plasmas of deuterium tritium in tokamaks", Ph.D. Thesis, Uppsala University (2000)

[13] L. Giacomelli *et al* , Eur. Phys. J. **D 33** (2005) 235

[14] H. Henriksson *et al* , Plasma Physics and Controlled Fusion **47** (2005) 1763

[15] G. Tardini *et al* , Journal of Instrumentation **7** (2012) C03004

[16] L. Giacomelli *et al* , Review of Scientific Instruments **82** (2011) 123504

[17] D. Marocco *et al* , IEEE Trans. Nucl. Sci. **56** (2009) 1168

[18] M. Riva *et al* , Fusion Eng. Des. **82** (2007) 1245

[19] V. Krasilnikov et al., Comp. Phys. Comm. **82** (2011) 735

[20] A. Pankin, D. McCune, R. Andre *et al*, Comp. Phys. Comm. **159**, No. 3 (2004) 157

[21] G. Tardini *et al* , Nuclear Fusion **53** (2013) 063027

[22] G. Tardini *et al* , Review of Scientific Instruments **87** (2016) 103504

[23] G. J. Wilkie *et al* , Plasma Physics and Controlled Fusion **59** (2017) 044007

[24] M. Reginatto, A. Zimbal, Review of Scientific Instruments **79** (2008) 023505

[25] R. Fischer *et al* , Proceedings of the Maximum Entropy Conference 1996, NMB Printers, Port Elizabeth, South Africa, 1997

[26] B. H. Park *et al* , Paper JP8.00122, Bull. Am. Phys. Soc. 54, (2012)

[27] M. Brambilla, Plasma Physics and Controlled Fusion **41** (1999) 1-34

[28] H. - S. Bosch, G. M. Hale, Nuclear Fusion **32** (1992) 611

[29] M. Nocente *et al* , Nuclear Fusion **51** (2011) 063011